



The magnetization reversal processes of $\text{Sm}_2\text{Gd}_{10.5}\text{Fe}_8\text{Co}_{64}\text{Zr}_{2.5}\text{Cu}_{13}$ alloy in the as-quenched state

M. Dospial^{a,*}, M. Nabialek^a, M. Szota^b, D. Plusa^a

^a Institute of Physics, Czestochowa University of Technology, 19 Armii Krajowej Av., 42-200 Czestochowa, Poland

^b Institute of Materials Science, Czestochowa University of Technology, 19 Armii Krajowej Av., 42-200 Czestochowa, Poland

ARTICLE INFO

Article history:

Received 2 July 2010

Received in revised form 6 December 2010

Accepted 7 December 2010

Available online 17 December 2010

PACS:

75.50.Tt

75.50.Ww

75.50.Vv

75.60.Jk

Keywords:

Permanent magnets

High coercivity materials

Magnetization reversal mechanisms

ABSTRACT

The magnetization reversal processes of the as-quenched $\text{Sm}_2\text{Gd}_{10.5}\text{Fe}_8\text{Co}_{64}\text{Zr}_{2.5}\text{Cu}_{13}$ ribbons obtained by melt-spinning method have been investigated. From the analysis of the initial magnetization curve it was deduced that the main mechanism of magnetization reversal process is the pinning of domain walls at the grain's boundaries. From the dependence of the reversible magnetization components as a function of magnetic field it was found that reversible rotation of magnetic moment vector results in high initial values of this component. The presence of several maxima on the differential susceptibility curves derived from the irreversible magnetization component in both direction of magnetization implies existence of several pinning sites for domain walls. The interaction between the alloy grains have been examined by using the so-called $\delta m(\mu_0 H_i)$ plot. The values of $\delta m(\mu_0 H)$ for investigated alloy remains positive for an applied field up to 1.15 T and negative for higher fields. Such behavior of $\delta m(\mu_0 H_i)$ dependence certifies that the dominant interaction between grains is the short range exchange interactions but low values of $\delta m(\mu_0 H)$ implies that these interactions are weak.

© 2010 Elsevier B.V. All rights reserved.

1. Introduction

The melt-spun Sm–Co type ribbons with close to the 1:7 composition displays interesting hard magnetic properties. The saturation magnetization $\mu_0 M_S$ of SmCo_7 alloys is relatively higher than composed of the SmCo_5 phase. They simultaneously possess high Curie temperature ($T_C \sim 1070$ K), strong uniaxial magnetocrystalline anisotropy field ($\mu_0 H_A \sim 9\text{--}19.2$ T at room temperature) and small temperature coefficient of coercivity β [1,2]. These features make magnets composed from the 1:7 type structures suitable for high temperature application.

The doping of Gd, Co, Fe, Zr, Hf, and Cu atoms to Sm–Co alloys allows to stabilize the TbCu_7 type structure and improve some magnetic properties in melt-spun ribbons [3]. The SmCo_7 alloys are metastable phases, their structure and magnetic properties depend strongly on processing techniques, heat treatment processes and doping elements [3–6].

In this article the investigation of the magnetization reversal processes of the as-quenched $\text{Sm}_2\text{Gd}_{10.5}\text{Fe}_8\text{Co}_{64}\text{Zr}_{2.5}\text{Cu}_{13}$ ribbons with the 1:7 type structure obtained by melt-spinning method has been performed. The sample was chosen from the

$\text{Sm}_x\text{Gd}_{12.5-x}\text{Fe}_8\text{Co}_{64}\text{Zr}_{2.5}\text{Cu}_{13}$ series as having the high coercivity in an as-cast state.

2. Materials and methods

2.1. Material

The $\text{Sm}_2\text{Gd}_{10.5}\text{Fe}_8\text{Co}_{64}\text{Zr}_{2.5}\text{Cu}_{13}$ samples were produced in the form of ribbons using a single roller melt-spinning method. The surface velocity of copper wheel was 40 $[\text{ms}^{-1}]$. The ingots were produced using high purity elements by the arc-melting of all components under a protective argon atmosphere. In order to obtain a homogeneous material, ingots were re-melted several times. The densities of the samples were estimated using Archimedes' law by a fluid displacement method. The samples (selected from different parts of the ribbon) were weighed ten times in air and toluene. Toluene was used, because of its well specified density variation with temperature. The deviation from the mean value was estimated using the Gauss method. The sample density was equal to 8.87 ± 0.09 g/cm^3 .

2.2. Experimental procedure

The phase composition of the as-quenched sample was verified using a "Bruker" X-ray diffractometer with a $\text{CuK}\alpha$ radiation source (1.541 Å) and a scintillation counter. The diffraction pattern was obtained for powdered sample using a fully automatic set-up at room temperature. The average grain size was estimated from ten Bragg's reflections with the highest intensities using the relation [7]:

$$\Delta^{hkl} (2\theta) \cos(\theta_B^{hkl}) = \frac{K\lambda}{D} + 2\varepsilon \sin(\theta_B^{hkl}) \quad (1)$$

where: D – grain size, K – shape factor, λ – X-ray wavelength, Δ^{hkl} is the line broadening at a half maximum intensity (FWHM) in radians, and θ_B^{hkl} is the Bragg angle.

* Corresponding author. Tel.: +48 34 3250610; fax: +48 34 3250795.

E-mail address: mdospial@wp.pl (M. Dospial).

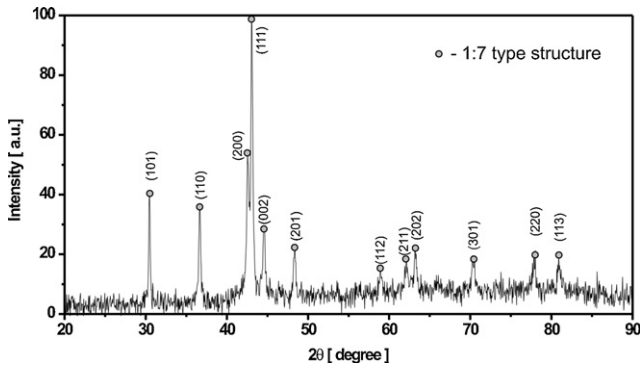


Fig. 1. X-ray diffraction pattern of melt-spun $\text{Sm}_2\text{Gd}_{10.5}\text{Fe}_8\text{Co}_{64}\text{Zr}_{2.5}\text{Cu}_{13}$ ribbon.

The relation (1) considers the effect of the grain size and strain on the half widths of the diffraction peaks.

The dependence (1) is linear and the grain size can be evaluated from the intersection of the straight line with the ordinate.

The magnetic measurements (the initial magnetization curve, the hysteresis loops and the recoil curves during magnetization and demagnetization process) at room temperature were performed using a Lake Shore vibrating sample magnetometer (VSM) under the influence of magnetic fields up to 2 T.

The data from all recoil loops in magnetization (demagnetization) direction have been used to derive the field dependence of the reversible $\mu_0 M_{\text{rev}}^r$ ($\mu_0 M_{\text{rev}}^d$) and irreversible $\mu_0 M_{\text{irr}}^r$ ($\mu_0 M_{\text{irr}}^d$) components of the total magnetization $\mu_0 M_{\text{tot}}^r$ ($\mu_0 M_{\text{tot}}^d$). The irreversible magnetization $\mu_0 M_{\text{irr}}^r$ ($\mu_0 M_{\text{irr}}^d$) is defined as the remanence when $\mu_0 H_i$ ($-\mu_0 H_i$) is changed to zero [8,9]. The reversible magnetization is the difference

$$\mu_0 M_{\text{rev}}^r(\mu_0 H_i) = \mu_0 M_{\text{tot}}^r(\mu_0 H_i) - \mu_0 M_{\text{irr}}^r(\mu_0 H_i) \quad (2)$$

The dependence of the reversible $\chi_{\text{rev}} = dM_{\text{rev}}/dH$ and irreversible $\chi_{\text{irr}} = dM_{\text{irr}}/dH$ components of total susceptibility $\chi_{\text{tot}} = dM_{\text{tot}}/dH$ on an applied magnetic field was also derived.

The interactions between grains were examined using $\delta m(\mu_0 H_i)$ plot derived from Wohlfarth's relation [10]:

$$\delta m(\mu_0 H_i) = \frac{\mu_0 M_{\text{irr}}^d(\mu_0 H_i)}{\mu_0 M_{\text{R}}} - \left(1 - 2 \frac{\mu_0 M_{\text{irr}}^r(\mu_0 H_i)}{\mu_0 M_{\text{R}}}\right) \quad (3)$$

where M_{R} is the remanence. For an assembly of noninteracting, single domain particles with uniaxial anisotropy the relation (3) is equal to 0. The deviation from the relation (3) was caused by the different kind of interactions between grains.

The VSM data were corrected for the demagnetizing field [11].

3. Results and discussion

Fig. 1 shows the XRD pattern of $\text{Sm}_2\text{Gd}_{10.5}\text{Fe}_8\text{Co}_{64}\text{Zr}_{2.5}\text{Cu}_{13}$ ribbon. The average grain size estimated from Eq. (1) was equal to $95 \text{ nm} \pm 1 \text{ nm}$, which means that the sample investigated belongs to the nanocrystalline materials. The results obtained from this pattern confirm that only one TbCu₇-type structure was present in the melt-spun ribbons.

Fig. 2 shows the initial magnetization curve and hysteresis loop measured in a field up to 2 T. The shape of the hysteresis loop points to a multi-phase material, containing six magnetic phases (not revealed by X-ray diffraction) with small and large coercivities (multi-stage demagnetization curve). The magnetic parameters determined from the hysteresis loop are as follows: the saturation magnetization $\mu_0 M_{\text{S}}(\infty) = 0.41 \text{ T}$ (after extrapolation to infinity field by the method described by Stoner and Wohlfarth using $\mu_0 M$ ($\mu_0 H$)⁻² dependence [12]), the remanence $\mu_0 M_{\text{R}}(2\text{T}) = 0.31 \text{ T}$ and the coercivity $\mu_0 H_{\text{CJ}}(2\text{T}) = 0.96 \text{ T}$.

As it can be seen in Fig. 2 the initial magnetization curve rises gradually and exhibit several inflection points. Such behavior results from the reversal magnetization mechanism dominated by the rotation of magnetic vector for lower and pinning of domain walls for higher values of an applied magnetic fields. The number of

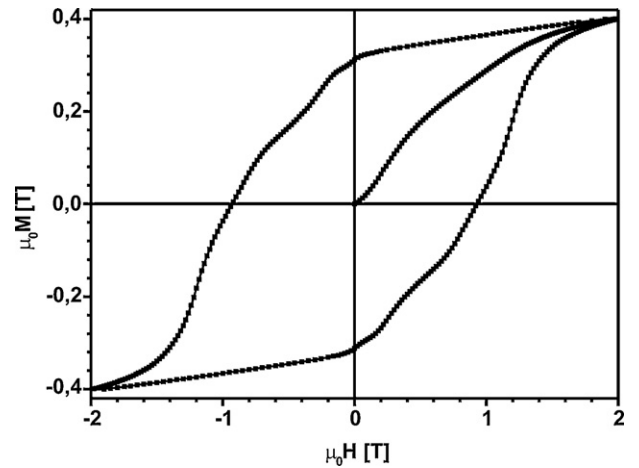


Fig. 2. Initial magnetization curve and hysteresis loop measured at 2 T external magnetic field.

inflection points present at the initial magnetization curve is related with number of pinning centers in alloy.

In order to understand better the coercivity mechanism in the investigated ribbons the recoil curves were measured in both magnetization directions. From these curves the reversible $\mu_0 M_{\text{rev}}$ and irreversible $\mu_0 M_{\text{irr}}$ components of the $\mu_0 M_{\text{tot}}$ magnetization were calculated (Fig. 3a and b).

It can be seen that the field dependence of the irreversible components in both magnetization direction are different. The irreversible component during the magnetization (demagnetization) is very low and hardly depends on internal magnetic field up to about 0.35 T (0.30 T). For higher fields $\mu_0 M_{\text{irr}}^r$ and $\mu_0 M_{\text{irr}}^d$ components increase faster and become greater then the reversible components at field 0.42 T and 0.77 T, respectively. The $\mu_0 M_{\text{irr}}^r$ ($\mu_0 H_i$) dependence has irregular shape and contains several inflection points. The $\mu_0 M_{\text{irr}}^d$ ($\mu_0 H_i$) dependence is more regular, two inflection points has been observed.

The magnetization changes are better seen in Fig. 4 which presents the reversible χ_{rev}^r (χ_{rev}^d) (Fig. 4a and b) and irreversible χ_{irr}^r (χ_{irr}^d) (Fig. 4c and d) differential susceptibility curves. Magnets in which the main magnetization reversal mechanism is connected with pinning of domain walls are characterized by a small initial value of the susceptibility and the maximum at a magnetic field close to the coercivity of the sample [13]. High values of the initial reversible susceptibility χ_{rev}^r (χ_{rev}^d) followed by rapid decrease in both magnetization directions (Fig. 4a and b) are connected with rotation of magnetic moments vectors. Presence of weak maxima at reversible magnetization curve (arrows indicating positions) close to the pinning field may be connected with bowing of pinned domain walls and motion of unpinned domain walls. The investigated melt-spun ribbon is characterized by the initial value χ_{irr}^r (χ_{irr}^d) close to zero and the presence of six maxima in both magnetization directions (Fig. 4c and d). Such a field dependence of the differential susceptibility implies the existence of six different pinning sites. The position of each maximum and its distribution were obtained by fitting the experimental points using six Gaussian distribution function. The percentage contribution of each pinning sites to the sample coercivity was determined from peak's area. These contributions are given in Fig. 4c and d. From these contributions using Eq. (4):

$$\mu_0 H_{\text{CJ}}^{r,d} = \sum_{n=1}^6 x_{\text{cn}} \frac{S_n}{S_{\text{tot}}} \quad (4)$$

where x_{cn} is position of the n -peak center, S_n – area of the n -peak and S_{tot} total area of fitted function, the coercivity of the sample was

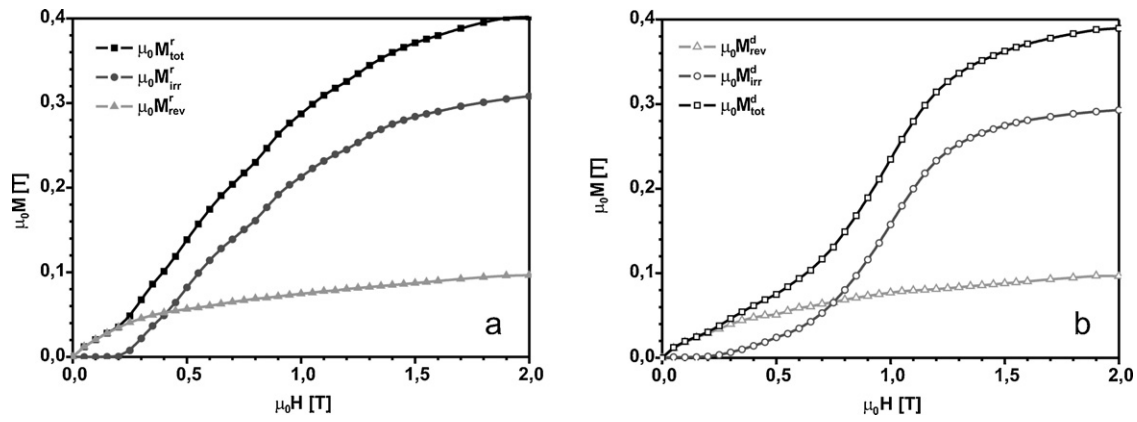


Fig. 3. Field dependence of the reversible and irreversible components of total magnetization during the initial magnetization (a) and the demagnetization (b).

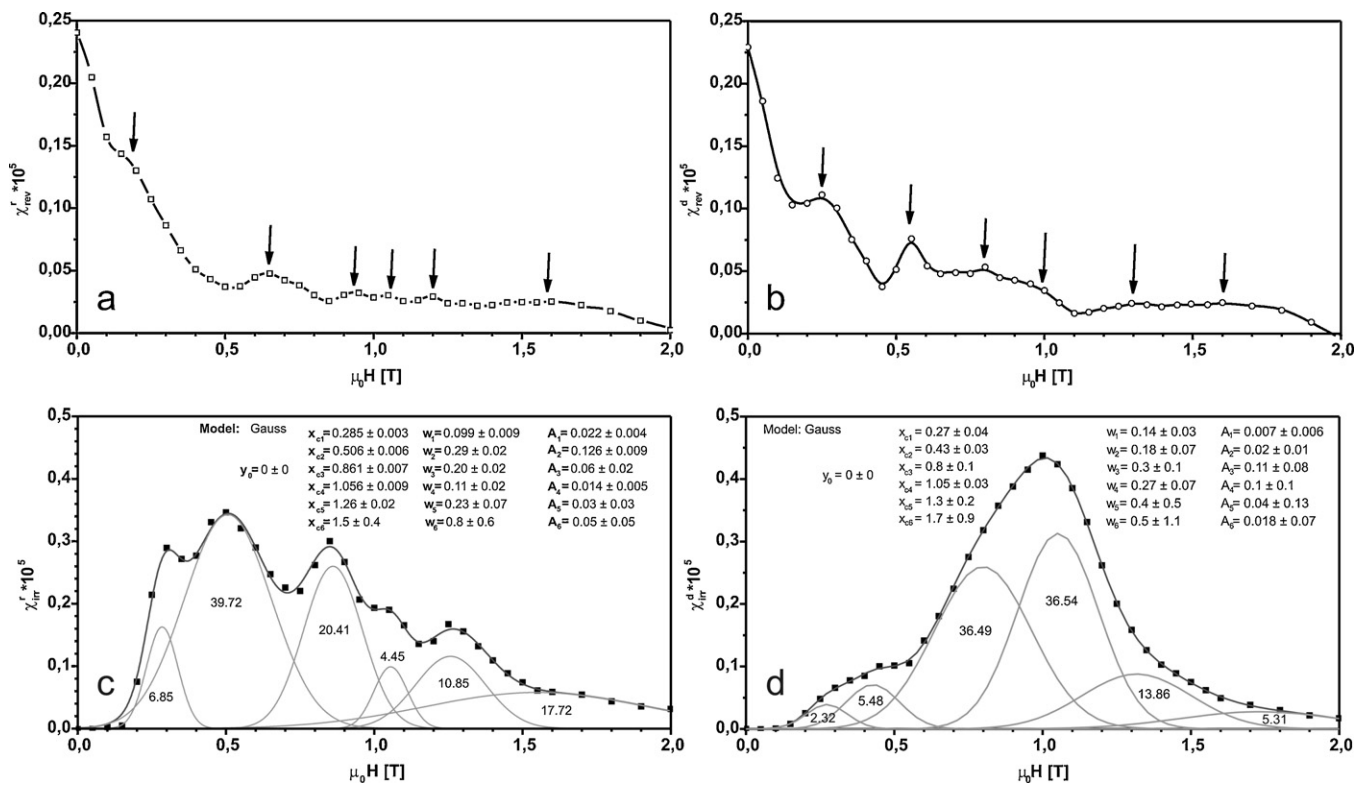


Fig. 4. Field dependence of the reversible (a and b) and irreversible (c and d) differential susceptibilities in magnetization and demagnetization direction, respectively.

estimated. It was found that estimated values of sample coertivity was equal 0.96 T for magnetization and 1.01 T for demagnetization direction, which corresponds approximately to the sample coercivity. Differences in obtained values may be connected with the fact that sample does not achieve the saturation at 2 T. The interaction between the alloy grains has been examined by use of the so-called $\delta m(\mu_0 H)$ plot described by Eq. (3) (Fig. 5) [14]: The interaction can be classified as long-range magnetostatic interaction and short-range exchange ones. For materials where interactions between particles are dominated by short-range exchange interactions (by long-range, dipolar interactions) δm plot remain positive (negative), respectively. The values of $\delta m(\mu_0 H)$ for investigated alloy remains positive for an applied field up to 1.15 T. Over this value $\delta m(\mu_0 H)$ becomes negative. $\delta m(\mu_0 H)$ plot implies that the dominant interaction between grains become short range

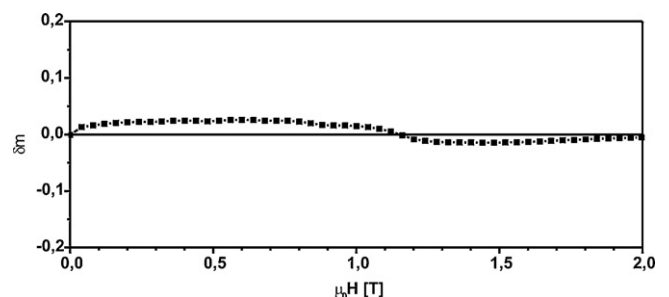


Fig. 5. $\delta m(\mu_0 H)$ plot of the melt-spun $\text{Sm}_2\text{Gd}_{10.5}\text{Fe}_8\text{Co}_{64}\text{Zr}_{2.5}\text{Cu}_{13}$ ribbon.

exchange interactions [15]. The low values of $\delta m(\mu_0 H)$ certifies that this interaction is very weak and does not cause the remanence enhancement.

4. Conclusions

The main magnetization reversal process in melt-spun $\text{Sm}_2\text{Gd}_{10.5}\text{Fe}_8\text{Co}_{64}\text{Zr}_{2.5}\text{Cu}_{13}$ alloy is the pinning of domain walls at structural inhomogeneities and grain boundaries. $\delta m(\mu_0 H)$ dependence results certifies that the dominant interaction between grains is the short range exchange interaction (S-shaped curve) but low values of $\delta m(\mu_0 H)$ implies that this interaction is very weak. This is confirmed by multi-stage shape of demagnetization curve, which should be smooth for a multi-phase magnets dominated by intergrain exchange interactions.

The high copper wheel velocity (40 m s^{-1}), allow to obtain melt-spun ribbons with fine grain size of the order of 95 nm.

References

- [1] K.H.J. Buschow, van der Goot, Acta Crystallogr. Sect. B: Struct. Crystallogr. Cryst. Chem. 27 (1971) 1085.
- [2] Y. Guo, W. Li, W. Feng, J. Luo, J. Liang, Q. He, X. Yu, Appl. Phys. Lett. 86 (2005) 192513.
- [3] M. Gjoka, O. Kalogirou, C. Sarafidis, D. Niarchos, G.C. Hadjipanayis, J. Magn. Magn. Mater. 242–245 (Part 2) (April 2002) 844–846.
- [4] M.Q. Huang, W.E. Wallace, M. McHenry, Q. Chen, B.M. Ma, J. Appl. Phys. 83 (1998) 6718.
- [5] M.Q. Huang, W.E. Wallace, M. McHenry, Q. Chen, B.M. Ma, J. Appl. Phys. 85 (1999) 5663.
- [6] M.Q. Huang, S.G. Sankar, W.E. Wallace, M. McHenry, Q. Chen, B.M. Ma, J. Appl. Phys. 87 (2000) 5305.
- [7] G.K. Willampson, W.H. Hall, Acta Metall. 1 (1953) 22.
- [8] C.L. Harland, L.H. Lewis, Z. Chen, B.-M. Ma, J. Magn. Magn. Mater. 271 (2004) 53.
- [9] R.W. Gao, D.H. Zhang, W. Li, X.M. Li, J.C. Zhang, R.W. Gao, D.H. Zhang, W. Li, X.M. Li, J.C. Zhang, J. Magn. Magn. Mater. 208 (2000) 239.
- [10] O. Henkel, Phys. Stat. Sol. (1964) 7919.
- [11] A.K. Panda, S. Basu, A. Mitra, J. Magn. Magn. Mater. 261 (1–2) (April 2003) 190–195.
- [12] E.C. Stoner, E.P. Wohlfarth, Trans. Roy. Soc. A240 (1948) 599.
- [13] E.P. Wohlfarth, J. Appl. Phys. 29 (1958) 595.
- [14] X.B. Du, H.W. Zang, C.B. Rong, J. Zhang, S.Y. Zhang, B.G. Shen, Y. Yan, H.M. Jin, J. Magn. Magn. Mater. 281 (2004) 255–260.
- [15] D. Plusa, B. Slusarek, M. Dospial, U. Kotlarczyk, T. Mydlarz, J. Alloys Compd. 423 (2006) 81–83.